

Travelling Fronts, Pulses, and Pulse Trains in a 1D discrete Reaction-Diffusion System

Priyadarshi Majumdar and Avijit Lahiri*

Dept of Physics, Vidyasagar Evening College, Kolkata 700 006, INDIA

Abstract

We follow up an earlier work (briefly reviewed below) to investigate the temporal stability of an exact travelling front solution, constructed in the form of an integral expression, for a one-dimensional discrete Nagumo-like model without recovery. Since the model is a piecewise linear one with an on-site reaction function involving a Heaviside step function, a straightforward linearisation around the front solution presents problems, and we follow an alternative approach in estimating a ‘stability multiplier’ by looking at the variational problem as a succession of linear evolution of the perturbations, punctuated with ‘kicks’ of small but finite duration. The perturbations get damped during the linear evolution, while the kicks amplify only the perturbations located at specific sites (the ‘significant perturbations’, see below) with reference to the propagating front. Comparison is made with results of numerical integration of the reaction-diffusion system whereby it appears likely that the travelling front is temporally stable for all parameter values characterising the model for which it exists. We modify the system by introducing a slow variation of a relevant recovery parameter and perform a leading order singular perturbation analysis to construct a pulse solution in the resulting model. In addition, we obtain (in the leading order) a 1-parameter family of periodic pulse trains for the system, modelling re-entrant pulses in a one-dimensional ring of excitable cells.

*Electronic address: a'l@vsnl.com

I. INTRODUCTION

The discrete Nagumo (FN) model [1] without recovery on a $1D$ lattice reads

$$\frac{du_n}{dt} = D(u_{n+1} - 2u_n + u_{n-1}) + f(u_n), \quad (1a)$$

where D is a diffusion constant coupling adjacent lattice sites and f is usually taken as a cubic bi-stable reaction function. It is considered relevant in numerous situations of interest, including the propagation of action potential along myelinated nerve axons, and excitations of cardiac cells (see [2, 3], and references in [1]). Following an earlier work [4] we consider a piecewise linear (PWL) version of (1a), with the reaction function given by

$$f(u) = -u - w + \Theta(u - a), \quad (1b)$$

where Θ stands for the Heaviside step function, the parameter a ($< 1/2$) is an effective threshold characterising each site, separating the equilibrium values 0 and 1 of the order parameter u_n , and w is a ‘recovery’ variable (see below). The model (1a), (1b) is essentially similar to the cubic Nagumo model in that each site is bi-stable in absence of the inter-site coupling. In [4] we gave an explicit construction of a travelling kink (or ‘front’) solution to this PWL version of the FN equations, of the form

$$u_n(t) = g(\zeta), \quad (2a)$$

where ζ is a propagation variable defined as $\zeta = (\chi t + n)$, χ being the speed of the propagating front. The profile function g was explicitly obtained as an integral expression

$$g(\zeta) = a_p + \int_0^\pi [b(\theta)e^{ip\theta} + b^*(\theta)e^{-ip\theta}]e^{-\lambda(\theta)(\zeta-p)} d\theta, \quad (2b)$$

where $p = [\zeta]$, the integer part of ζ , and

$$a_p = 1 - w - \frac{\gamma}{1 + \gamma} \gamma^p \quad (p \geq 0), \quad (3a)$$

$$= -w + \frac{1}{1 + \gamma} \gamma^{-p} \quad (p \leq 0), \quad (3b)$$

$$b(\theta) = -\frac{1}{2\pi} \frac{1}{2D + 1} \frac{1}{1 - \nu \cos \theta} \frac{1}{1 - e^{-i\theta} e^{-\mu(1 - \nu \cos \theta)}}, \quad (4)$$

$$\lambda(\theta) = \frac{1}{\chi} (2D \cos \theta - (2D + 1)). \quad (5)$$

Here the parameters γ , μ , ν are defined as

$$\gamma \equiv 1 + \frac{1}{2D} - \sqrt{\left(\frac{1}{D} + \frac{1}{4D^2}\right)}, \quad (6a)$$

$$\mu \equiv \frac{2D+1}{\chi}, \quad (6b)$$

$$\nu \equiv \frac{2D}{2D+1}. \quad (6c)$$

The speed χ gets determined through a matching condition, for which we refer to [4]. An important observation is that, in contrast to a continuously distributed excitable medium, a travelling front on a discrete lattice gets *pinned* (in this context, see [1, 5]) as the threshold approaches a certain limiting value \tilde{a} (see [4]) where

$$\tilde{a} = -w + \frac{1}{2}\left[1 - \sqrt{\left(\frac{1}{1+4D}\right)}\right] < \frac{1}{2} - w. \quad (7)$$

For a 1D continuously distributed reaction-diffusion system with the same reaction function as in eq. (1b) a travelling kink solution would exist, for any given D , for all values of the threshold parameter in the range $0 < a < \frac{1}{2} - w$.

The above explicit solution was obtained in [4] by noting that, as the front propagates, there occur successive time intervals (equivalently, intervals in ζ) during which the system (1a), (1b) evolves linearly, and the transition from one interval to the next is marked by the value of u_n crossing the threshold for some appropriate site n . The full solution is then obtained by an appropriate matching at these transition points between superpositions of the eigenmodes of the linear system.

Fig. 1 shows the pulse profile $g(\zeta)$ for arbitrarily chosen values of a , D , where one observes that $g(\zeta)$ is piecewise continuous, with a discontinuous derivative at each lattice site owing to the presence of the Heaviside step function in the model (we choose the origin of time such that u_0 crosses the threshold a at $t = 0$ and, accordingly, u_n crosses the threshold at $t = -\frac{n}{\chi}$).

In the first part of this paper we present a stability analysis of the travelling front (eq. (2a), (2b))(see [6, 7] for an early work demonstrating the existence of stable travelling wave solutions for the Nagumo model), arriving at an estimate of a certain ‘stability multiplier’ ρ (see below) which is to be less than unity for the front solution to be stable, and show

numerically that conclusions arrived at on the basis of this multiplier are indeed conformed to in the actual time evolution of the FN system under consideration. The presence of the Heaviside function in the model makes the linearised evolution equation singular, involving delta functions at the transition points referred to above, and so a straightforward calculation of the linear growth rates cannot be attempted in the model.

In section 2, we circumvent this difficulty by looking more closely at the evolution of perturbations imposed on (2a), (2b), and estimate the stability multiplier, thereby arriving at the conclusion that the travelling front solution obtained in [4] is stable.

In section 3 we indicate that the system (1a), (1b) involves a certain symmetry, whereby an ‘anti-kink’ solution is associated with a kink solution for any given w . We then modify the system (1a), (1b) by including an equation representing the slow evolution of the recovery variable w , and perform a leading order singular perturbation analysis whereby a kink and a corresponding anti-kink solution are pieced together to yield a travelling *pulse* solution of the modified system. We also indicate how a *pulse train* solution involving an infinite periodic array of uniformly propagating pulses can be obtained in the model.

Section 4 is devoted to concluding remarks, with brief mention of a future communication relating to the stability of the pulse solution.

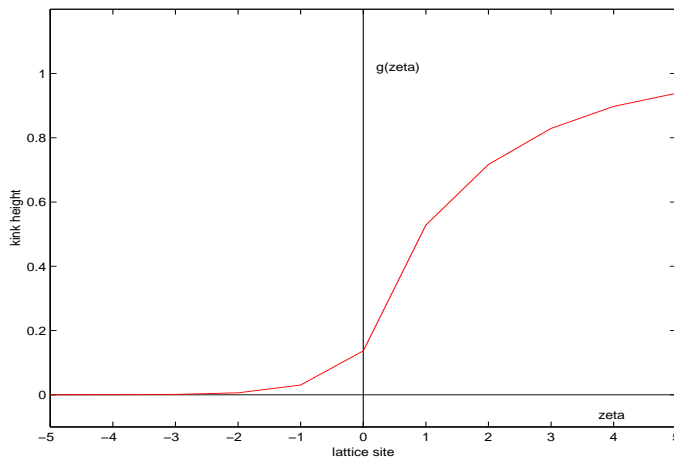


FIG. 1: Kink profile function $g(\zeta)$ showing discontinuity of derivative at integer values of the propagation variable ζ (corresponding to integers representing lattice sites at $t = 0$); parameter values are $w = 0, D = 1, a = 0.1382$.

II. STABILITY OF THE TRAVELLING FRONT: THE STABILITY MULTIPLIER

As mentioned above, a straightforward linearisation around the travelling front solution presents technical problems involving the appearance of delta functions that make the linearised equations more singular than they actually are. Instead, if we look at the time evolution of a perturbation over the front solution in accordance with (eq. (1a), (1b)), we find that this involves a succession of intervals of linear evolution, punctuated by ‘kicks’ at the transition points wherein the evolution involves a difference between two step functions - one with and the other without the perturbation. For small perturbations one can then make a convenient approximation giving the evolution of the perturbation through the kick.

More precisely, denoting by $\eta_n(t)$ the perturbation over the travelling kink soln. $u_n(t)$ (eq. (2a), (2b)), the time evolution of η_n is given by

$$\frac{d(\eta_n(t))}{dt} = D(\eta_{n+1}(t) - 2\eta_n(t) + \eta_{n-1}(t)) - \eta_n(t) + \Theta(u_n(t) + \eta_n(t) - a) - \Theta(u_n(t) - a). \quad (8)$$

For given n , $u_n(t)$ crosses the threshold a at $t = t_n \equiv -\frac{n}{\chi}$. Thus, assuming, for instance, $\eta_n(t)$ to be positive, we have

$$\Theta(u_n + \eta_n - a) - \Theta(u_n - a) = 1 \quad (9a)$$

for

$$a - \eta_n < u_n(t) < a, \quad (9b)$$

and zero otherwise.

In the following, the time interval during which this inequality holds will be termed a ‘kick’. As will be seen below, η_n increases monotonically during the kick and hence the kick begins when

$$u_n(t) = a - \eta_n^-, \quad (10)$$

η_n^- being the value of η_n just before the kick.

Now, for t sufficiently close to but less than t_n ,

$$u_n(t) = a + \dot{u}_n(t_n^-)(t - t_n) + O(|t - t_n|^2), \quad (11)$$

where $\dot{u}_n(t_n^-)$ is used by recalling that \dot{u}_n is actually discontinuous at $t = t_n$. Thus, for η_n sufficiently small,

$$u_n(t) = a - \eta_n^- \quad (12a)$$

for

$$t \approx t_n - \frac{\eta_n^-}{\dot{u}_n(t_n^-)}, \quad (12b)$$

where we have assumed that $\dot{u}_n(t_n^-)$ is not so small as to make the term $O(|t - t_n|^2)$ relevant in (11).

Thus, the time interval during which $(\Theta(u_n + \eta_n - a) - \Theta(u_n - a))$ differs from zero, ranges from $(t_n - \frac{\eta_n^-}{\dot{u}_n(t_n^-)})$ to t_n . This time interval we have designated above as a ‘kick’. The time evolution of $\eta_n(t)$, ($n = 0, \pm 1, \pm 2, \dots$) is then one involving a series of kicks, punctuated by intervals where the difference of Θ -functions in (8) is zero, during which we have

$$\frac{d\eta_n}{dt} - D((\eta_{n+1}(t) - 2(\eta_n(t) + \eta_{n-1}(t)) + \eta_n(t)) = 0. \quad (13)$$

For sufficiently small η_n ’s the kicks are short-lived, and of an impulsive nature. Thus, during the n th kick we have, to a good degree of approximation,

$$\frac{d\eta_n}{dt} = 1, \quad (14)$$

while the other η_m ’s remain almost unaffected during this short interval. In between kicks, the perturbation evolves according to (13). Equation (14) tells us that η_n indeed increases monotonically during the kick, and the values of η_n just before and just after the n th kick are related as

$$\eta_n^+ = \eta_n^- + \tau_n, \quad (15)$$

where τ_n is the duration of the kick.

Finally, using (12b) one gets,

$$\eta_n^+ = \left(1 + \frac{1}{\dot{u}_n(t_n^-)}\right) \eta_n^-, \quad (16)$$

or, using the profile function $g(\zeta)$ and noting that

$$\dot{u}_n(t_n^-) = \chi g'(\zeta)|_{\zeta=0^-}, \quad (17)$$

we obtain,

$$\eta_n^+ = \left(1 + \frac{1}{\chi g'(0^-)}\right) \eta_n^-. \quad (18)$$

We note in passing that a straightforward linearisation through the replacement of $(\Theta(u_n + \eta_n - a) - \Theta(u_n - a))$ by $\delta(u_n - a)\eta_n$ would give us

$$\eta_n^+ = e^{\frac{1}{\chi g'(0^-)}} \eta_n^-, \quad (19)$$

and would make the problem more singular than it actually is. In other words, even for small η_n , one has to take into account the non-linearity during the interval occupied by the kick, while retaining only the linear term in the *duration* of the kick.

In a similar manner, if η_n^- happens to be negative, one finds

$$\eta_n^+ = \frac{1}{1 - \frac{1}{\chi g'(0^+)}} \eta_n^-. \quad (20)$$

The difference between (18) and (20) is once again a reflection of the fact that the non-linearity is relevant during the interval of the kick.

In the following we present an approximate stability analysis by estimating what we have termed the ‘stability multiplier’ and our conclusions are essentially independent of whether we use (18) or (20) for the amplifying effect of the kick on the perturbation. For the sake of simplicity we use below eq. (18) in so far as the effect of the kick is concerned.

We now look into eq. (13) to see what happens to the perturbation in between the kicks. This is a system of linear equations and can be easily integrated for a time interval $\tau = \frac{1}{\chi}$ from, say, the end of one kick and the beginning of the next:

$$\eta_m(t + \tau) = e^{-(2D+1)\tau} \sum_m I_{n-m}(2D\tau) \eta_m(t), \quad (21)$$

where I_l stands for the Bessel function of order l with imaginary argument:

$$I_l(u) = \frac{1}{2\pi} \int_0^{2\pi} e^{u \cos \theta} e^{il\theta} d\theta. \quad (22)$$

One can also check that evolution through (13) leads to an over-all damping of the perturbation as expected and, for instance, obtain the following bound,

$$\sum_n |\eta_n(t + \tau)|^2 \leq e^{-2\tau} \sum_n |\eta_n(t)|^2. \quad (23)$$

Indeed, all the eigenvalues of the linear problem are real and negative, giving us the result (23).

We now piece together the results obtained above. Starting from time, say 0^+ , just after the kick at the site $n = 0$ (recall that a kick affects the perturbation at one site only, leaving unchanged the other sites), the perturbation decays through linear evolution till the next kick arrives at $t_{-1} = \frac{1}{\chi}$. There follows the impulsive action of the kick, amplifying the perturbation at site $n = -1$ by the factor on the right hand side of (18), leaving the perturbation at the other sites unchanged. The process is repeated thereafter, the site of action of the kick being shifted successively by one lattice site.

Note that, with the shift of the site of action of the kick the front itself, represented by (2a), (2b), moves through one lattice site during the linear evolution. Since the kick at $n = 0$ occurs at $t_0 = 0$ when the front is also located at $n = 0$, we conclude that *each kick amplifies the perturbation precisely at that lattice site where the front is located at that instant*. Since the linear evolution uniformly damps out the perturbations, we see that the most crucial factor in respect of the time evolution of the perturbation resides in the answer to the question: what happens to the perturbation *at the site of location of the front* as the latter propagates along the lattice? Since the perturbations at the other lattice sites are not affected by the kicks, they are damped out.

Thus, focussing on the perturbation at the location of the front (we call it the ‘significant perturbation’) as it gets shifted from site to site, we calculate the factor through which it gets amplified during the interval of one kick and the subsequent linear evolution till the arrival of the next kick, and call it the *stability multiplier*. The latter is made up of two factors, of which one is given by eq. (18). The other factor is to be obtained from eq. (21) as the effect of the linear evolution on the significant perturbation.

One observes, for instance, that at the end of the time interval (of length $\tau = \frac{1}{\chi}$) from t_0^+

(end of kick at site $n = 0$) up to t_{-1}^- (begining of kick at site $n = -1$) the perturbation at site $n = -1$ (the significant perturbation at time t_{-1}) depends linearly on the perturbations at the various sites at time t_0^+ (i.e. the time of the previous kick). Among the latter, the one at site $n = 0$ (i.e. the significant perturbation at time t_0) is of largest magnitude and happens to have the maximum effect on the perturbation at site $n = -1$ at time $t_{-1} = \tau = \frac{1}{\chi}$ because of its proximity.

Thus, in order to have an order of magnitude estimate of the stability multiplier, we make the simplification of ignoring all perturbations on the right hand side of eq. (21) excepting the one with $m = -1$ which gives, for instance,

$$\eta_{-1} = e^{-(2D+1)\tau} I_1(2D\tau)\eta_0(0^+). \quad (24)$$

Noting that η_0 and η_{-1} are the significant perturbations at $t = 0$ and $t = \tau$ respectively, we conclude that the second factor in the stability multiplier arising due to the linear evolution is $e^{\frac{-(2D+1)}{\chi}} I_1(\frac{2D}{\chi})$.

Thus, finally we arrive at the required estimate of the stability multiplier

$$\rho = \left(1 + \frac{1}{\chi g'(0^-)}\right) e^{\frac{-(2D+1)}{\chi}} I_1\left(\frac{2D}{\chi}\right) \quad (25a)$$

$$= \frac{1}{2\pi} \left(1 + \frac{1}{\chi g'(0^-)}\right) e^{\frac{-(2D+1)}{\chi}} \int_0^{2\pi} e^{\frac{2D}{\chi} \cos\theta} \cos\theta d\theta. \quad (25b)$$

Making use of the multiplier ρ , we arrive at the stability criterion,

$$\rho < 1. \quad (26)$$

In reality, eq. (26) is not an exact criterion because (i) eq. (18) is not an exact amplification factor due to a kick since it is valid for only one class of perturbations; (ii) it is based on an approach that looks at the evolution of the significant perturbation alone; and, (iii) so far as the effect of the linear evolution on the significant perturbation is concerned, eq. (24) overlooks perturbations at all sites excepting the significant one at the previous kick.

Still, one can look upon eq. (25a) as an effective stability criterion, that can be used as a convenient guide in assessing the linear stability of the propagating front solution (eq. (2a), (2b)) of the FN system (eq. (1a), (1b)) under consideration. As we indicate below, numerical computations conform quantitatively to conclusions arrived at from eq. (25a).

While accepting eq. (25a) as a stability criterion one, however, has to make a couple of qualifications relation to its validity in the limits $\chi \rightarrow 0$ (pinning limit) and $\chi \rightarrow \infty$ (zero threshold, see [4]). Indeed, making use of results in [4] and of the asymptotic properties of Bessel functions, one finds, in the pinning limit $\chi = 0$,

$$1 + \frac{1}{\chi g'(0^-)} \rightarrow \frac{\sqrt{4\pi D}}{\sqrt{\chi}} e^{\frac{1}{\chi}}, \quad (27a)$$

$$e^{-\frac{2D+1}{\chi}} I_1\left(\frac{2D}{\chi}\right) \rightarrow \frac{\sqrt{\chi}}{\sqrt{4\pi D}} e^{-\frac{1}{\chi}}, \quad (27b)$$

i.e., in the pinning limit, we have,

$$\rho \rightarrow 1. \quad (28)$$

On the other hand, in the limit $\chi \rightarrow \infty$, one similarly has,

$$1 + \frac{1}{\chi g'(0^-)} \rightarrow \frac{\chi}{D}, \quad (29a)$$

$$e^{-\frac{2D+1}{\chi}} I_1\left(\frac{2D}{\chi}\right) \rightarrow \frac{D}{\chi}, \quad (29b)$$

i.e., once again,

$$\rho \rightarrow 1. \quad (29c)$$

Thus, on the face of it, our theory makes no definite predictions regarding stability in the pinning limit as also the limit of infinitely fast kinks.

However, in both these limits, one notes that the amplification factor due to the kick given by (18) goes to infinity. This, in fact, is an overestimate since for $g'(0^-) \rightarrow 0$, the second term in (11) becomes vanishingly small and the third term, involving $g''(0^-)$ is to be taken into account, and thus the expression for the kick duration

$$\tau_n = \frac{\eta_n^-}{\chi g'(0^-)}, \quad (30)$$

is an over-estimation. On the other hand, the damping factor due to linear evolution does go to zero in both these limits, and hence stability is recovered for both $\chi \rightarrow 0$ and $\chi \rightarrow \infty$.

On the other hand, for front speeds neither too small nor too large, expression (25a) can be taken as a correct order-of-magnitude estimate. Using the front solution (2a), (2b), one can compute ρ for given values of parameters a and D characterising the system.

In fig. 2, we show the variation of the stability multiplier ρ with a for a set of different values

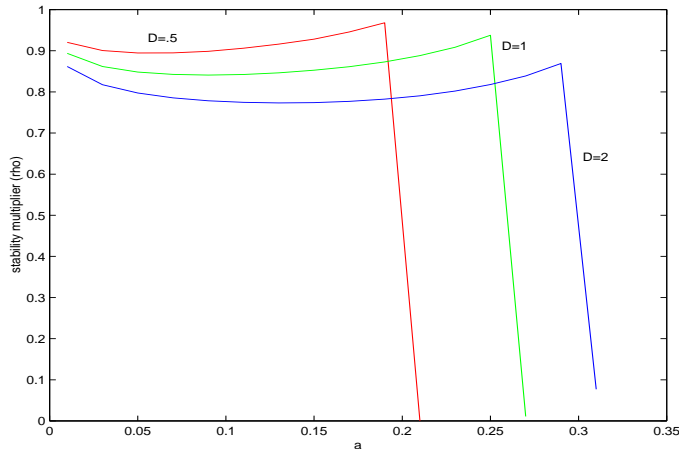


FIG. 2: Stability multiplier ρ as a function of the threshold parameter a for various different values of D . Fall of ρ near the limiting value \tilde{a} ($\chi \rightarrow 0$) is an artefact (see text).

of D where we find that $\rho < 1$ for the entire range of parameter values except for $a \rightarrow 0$ ($\chi \rightarrow \infty$) when one has $\rho \rightarrow 1$ in accordance with (29c) (one finds in this figure that $\rho \rightarrow 0$ in the pinning limit $a \rightarrow \tilde{a}$ in apparent violation of (28); however, this is an artefact because the program used to evaluate (27a) yields an underestimation, failing to reproduce the exponential divergence). As already mentioned, (28), (29c) are overestimations in relation to the actual value of ρ in these two limits. In other words, the travelling front solution obtained in our model is stable for all the parameter values for which it exists. This conclusion is confirmed from fig. 3 where we show the variation of a related multiplier $\tilde{\rho}$ (see below) with a , again for a set of different values of D . We obtain $\tilde{\rho}$ as follows: we impose a perturbation η_0 on the travelling front located at the site $n = 0$ at time $t = 0$, and allow the perturbed system to evolve for a time $\tau = \frac{1}{\chi}$, following the evolution through numerical integration. At the end of this interval, we look at the perturbation η_{-1} at site $n = -1$. The ratio $\frac{\eta_{-1}}{\eta_0}$ is then

defined as $\tilde{\rho}$, which is thus a numerical estimate for the stability multiplier ρ determined from the actual time evolution of the system under consideration.

A comparison of figures 2, 3 shows that the variations of ρ , $\tilde{\rho}$ are similar in nature (excepting for small a , see above), indicating that our theoretical estimate gives qualitatively correct predictions relating to the stability of the propagating front, and the front solution is indeed stable in its entire range of existence.

Fig. 4 presents results of numerical integration of (1a), (1b) for more general perturbations. We impose over the kink profile a perturbation spread over a few sites around $n = 0$ at $t = 0$ (recall that this includes what we have termed the significant perturbation) and look at the front profile after an appropriate time interval to see what has happened to the perturbation. It is found that, for all values of the parameters a , D for which the integration is performed (only a few representative ones among these are shown in fig. 4) the perturbation dies down with time.

In summary, we conclude that the stability multiplier ρ obtained above gives a reliable indication of the temporal stability of the travelling front solution and that the latter is, in all likelihood, stable for all values of the parameters a , D for which it exists.

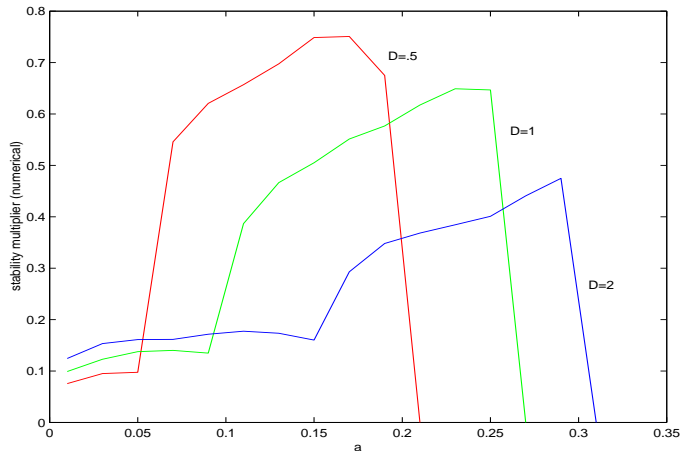


FIG. 3: Stability multiplier $\tilde{\rho}$ obtained from numerical integration of the Nagumo system (see text) as a function of a for different values of D ; compare with fig. 2.

III. THE PROPAGATING ANTI-KINK, PULSE, AND PULSE-TRAIN SOLUTIONS

A. The anti-kink

We begin by noting that equations (1a), (1b) possess a symmetry $w_n \rightarrow 1 - 2a - w_n$, $u_n \rightarrow 2a - u_n$, as a result of which there is associated, with a travelling front or kink solution, a travelling ‘anti-kink’ propagating with the same speed χ . The latter is obtained from the former, equations (2a), (2b), by making the above transformation. Fig. 5 depicts schematically the level change in u_n (for a given lattice site n) for the kink and the corresponding anti-kink solution, the level change for the latter being shown in such a manner that both the kink and the anti-kink propagate in the same direction along the lattice.

B. Fast and slow dynamics: the travelling pulse solution

We now modify our system (1a), (1b) in such a way that there occurs a slow change in the recovery variable w_n as a result of which, after the level change in u_n in the kink solution (for

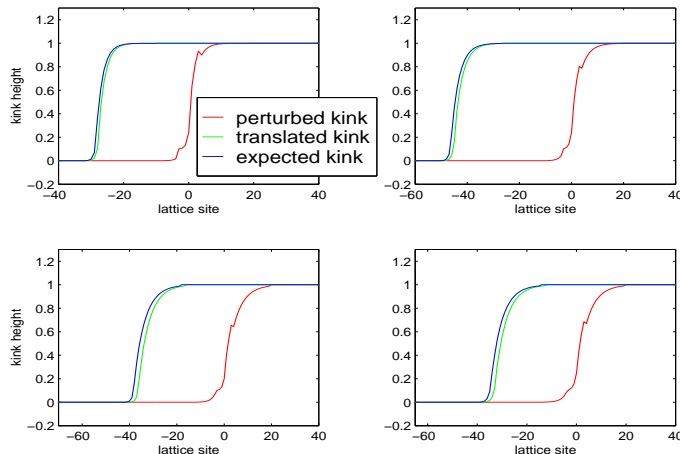


FIG. 4: Numerical integration of the Nagumo system for an initial kink solution together with a perturbation; clockwise from top left (a) $D = 1, a = 0.1382, \tau = 20$, (b) $D = 2, a = 0.1, \tau = 20$, (c) $D = 3, a = 0.1445, \tau = 10$, (d) $D = 4, a = 0.2272, \tau = 10$; in each frame, the profile obtained through numerical integration for a time τ (‘translated kink’) has been compared with the profile obtained from the theoretically obtained solution with $t = \tau$ (‘expected kink’).

any given n , with $w_n = 0$) from a low to a high level (with reference to the threshold a), there occurs a slow rise in w_n and a corresponding slow fall in u_n till there appears a rapid level change in u_n in accordance with the anti-kink solution matching the earlier kink solution, now with $w_n = 1 - 2a$. Thereafter, there occurs a slow change in w_n and u_n whereby both return to the resting value 0. Such alteration of fast and slow dynamics is actually observed in excitable media of interest, and provides the basis for FitzHugh-Nagumo dynamics (see, e.g., [8]) as a prototype model for such systems.

In an early paper, Conley [9] gave a geometric argument based on a singular perturbation approach where he established the existence of a homoclinic orbit representing a pulse solution (in the context of a 1D continuous excitable medium) on reducing the partial differential equations to a system of ODE's in terms of an appropriate propagation variable. Such pulse solutions in spatially continuous systems have since been extensively discussed in the literature (see, e.g., [10, 11, 12, 13]). In particular the question of stability of these pulses, obtained by piecing together a leading front and a trailing rear (respectively the 'kink' and the 'anti-kink'), has been addressed in the context of the so-called restitution hypothesis [14, 15].

In the following, we present a leading order singular-perturbation construction, along similar

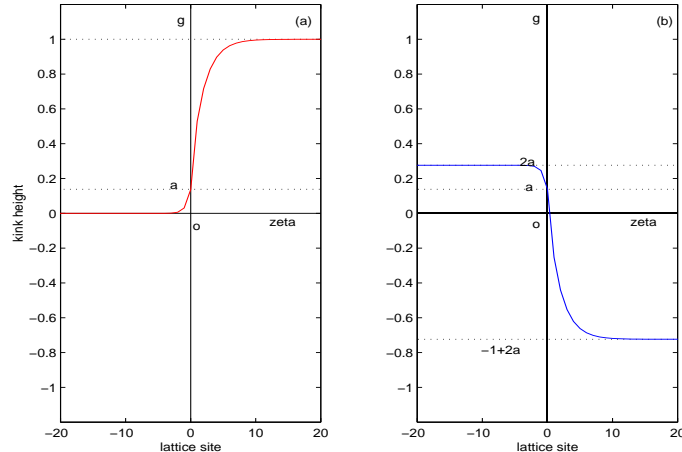


FIG. 5: The (a) kink and (b) anti-kink profiles as function of ζ (corresponding to integers representing lattice sites at $t = 0$) showing level changes for given $D(= 1)$ and $a(= 0.1382)$; introduction of the slow dynamics connects up the kink and the anti-kink into a travelling pulse (see text).

lines, of the pulse solution in a 1D *discrete* lattice in the above-mentioned modification of the system (1a), (1b) obtained by introducing the slow dynamics involving the recovery variable w_n . More precisely, the system we now consider is

$$\frac{du_n}{dt} = D(u_{n+1} - 2u_n + u_{n-1}) + f(u_n), \quad (31a)$$

$$\frac{dw_n}{dt} = \epsilon u_n, \quad (31b)$$

where ϵ is a small recovery parameter setting the time scale of the slow dynamics in terms of which we perform below the leading order singular perturbation calculation.

We now have two pieces of inner solution describing a rapid level change in u_n (for $w_n = 0$ and $w_n = 1 - 2a$ for the kink and the anti-kink respectively) and two other pieces of outer solution involving the slow change of u_n as also of w_n . Fig. 6 shows schematically the variation of u_0 with t in which ABC depicts the leading edge and DE the trailing edge while CD and EF correspond to the slow dynamics. The points C, D, and E indicate the points of matching between the inner and outer solutions, which we work out below. Fig. 7 depicts the pulse solution in the u_0 - w_0 (the choice $n = 0$ is arbitrary) phase plane, where the matching points are indicated once again, together with the points B, D' where u_0 crosses the threshold with $w_0 \approx 0$ and $w_0 \approx 1 - 2a$ respectively. Note that the pulse rises from $u_0 = 0$ at $t \rightarrow -\infty$ and finally recovers to $u_0 = 0$ at $t \rightarrow +\infty$. Thus, from here on, we denote by $g(\zeta)$ the kink solution described in section 1, *with the recovery parameter w set at 0* (the same notation will apply for the pulse-train solution as well).

Following [4] we introduce the propagation variable $\zeta = \chi t + n$, and represent the pulse solution as

$$u_n(t) = u(\zeta), \quad (32a)$$

$$w_n(t) = w(\zeta), \quad (32b)$$

where

$$\lim_{\zeta \rightarrow \pm\infty} u(\zeta) = \lim_{\zeta \rightarrow \pm\infty} w(\zeta) = 0. \quad (32c)$$

Let the values of the propagation variable at the matching points be denoted by ζ_C , ζ_D , and ζ_E respectively, which we calculate below in the leading order in ϵ .

Starting from the kink solution (2a), (2b), for $\epsilon = 0$, $w = 0$, one obtains the leading correction as we switch on a small ϵ :

$$w(\zeta) = \frac{\epsilon}{\chi} \int_{-\infty}^{\zeta} g(\zeta) d\zeta. \quad (33)$$

Noting that $g(\zeta) \sim 0$ (here and in the following we use the symbol ‘ \sim ’ to denote a leading order approximation in ϵ) for ζ away from and less than 0, while $g(\zeta) \sim 1$ for ζ greater than and away from 0, we get the asymptotic expression for $w(\zeta)$ for large ζ :

$$w(\zeta) \sim \frac{\epsilon\zeta}{\chi}. \quad (34)$$

With this as the inner solution for w for $0 < \zeta < \zeta_C$, and the corresponding inner solution for u as

$$u(\zeta) \sim g(\zeta), \quad (35)$$

the *outer* solution satisfies, from eq. (31a),

$$u(\zeta) \sim 1 - w(\zeta). \quad (36a)$$

where, from (31b)

$$w(\zeta) \sim 1 - e^{-\frac{\epsilon}{\chi}\zeta}. \quad (36b)$$

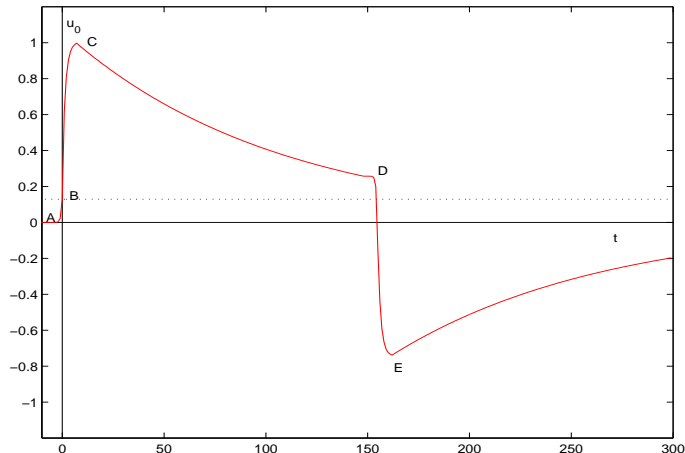


FIG. 6: u_0 as a function of t for a typical pulse solution showing schematically the points of matching between the fast and slow dynamics; the choice $n = 0$ for the lattice site is arbitrary.

Matching the inner and outer solutions, we get the value of ζ_C from

$$g(\zeta_C) \sim 1 - \frac{\epsilon \zeta_C}{\chi}. \quad (37)$$

It is now necessary to obtain the asymptotic expression for $g(\zeta)$ for large $|\zeta|$ in order to solve for ζ_C from above. This can be done by noting that, in the asymptotic region, the linear approximation holds for the evolution of $u_n(t)$, i.e.,

$$\chi \frac{dg(\zeta)}{d\zeta} = D(g(\zeta + 1) - 2g(\zeta) + g(\zeta - 1)) - g(\zeta) + g_0, \quad (38)$$

where $g_0 = 1$ (resp. 0) for $\zeta \rightarrow +\infty$ (resp. $\zeta \rightarrow -\infty$). Then, assuming

$$g(\zeta) - g_0 \sim \sigma^{|\zeta|} \text{ (say)}, \quad (39)$$

we have,

$$\chi \ln \sigma = D(\sigma + \sigma^{-1}) - (2D + 1), \quad (40)$$

from which one can determine the exponent σ . As an example, we have the results

$$\sigma = \gamma, \quad \text{for } \chi \rightarrow 0, \quad (41)$$

and

$$\sigma = e^{-\frac{1}{\chi}}, \quad \text{for } \chi \rightarrow \infty, \quad (42)$$

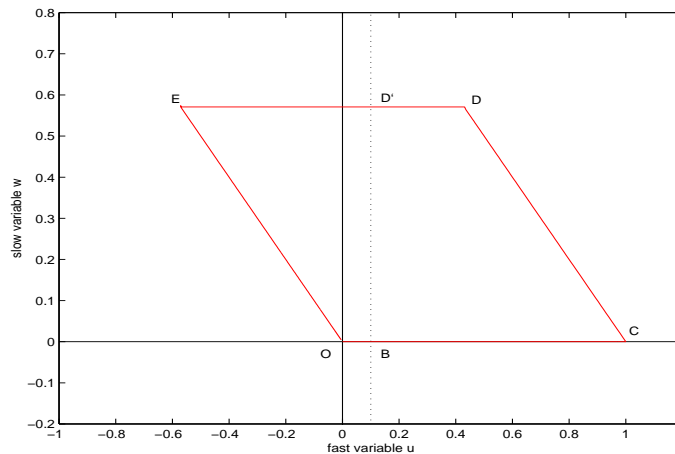


FIG. 7: u_0-w_0 (the choice $n = 0$ for the lattice site is arbitrary) phase diagram for the pulse solution showing points of matching as also the points where u_0 crosses the threshold a ; the origin (O) is the asymptotic point for the orbit for $t \rightarrow \pm\infty$.

i.e.,

$$g(\zeta) = g_0 + \alpha\gamma^{|\zeta|}, \quad \text{for } \chi \rightarrow 0, \quad (43)$$

and

$$g(\zeta) = g_0 + \beta(e^{-\frac{1}{\chi}})^{|\zeta|}, \quad \text{for } \chi \rightarrow \infty, \quad (44)$$

where α, β are constants whose values need not concern us here.

Thus, in the following, we write $g(\zeta) = g_0 + A\sigma^{|\zeta|}$ for $|\zeta| \rightarrow \infty$ for arbitrarily specified χ, D , where the constant A is not relevant for our analysis, and where σ is to be determined from the transcendental equation (40).

Thus, finally, the matching at the point C gives (ref. eq. (37))

$$1 + A\sigma^{\zeta_C} = 1 - \frac{\epsilon\zeta_C}{\chi}, \quad (45)$$

giving,

$$\zeta_C \sim \frac{\ln\epsilon}{\ln\sigma}. \quad (46)$$

Next, it is easy, from (36b), to calculate to leading order in ϵ the time or ζ -interval from C to D, the latter being the point where $w(\zeta) \sim 1 - 2a$. One thereby gets

$$\zeta_D - \zeta_C \sim \frac{\chi}{\epsilon} \ln\left(\frac{1}{2a}\right). \quad (47)$$

As expected, the interval (ζ_C) after which the fast dynamics is succeeded by the slow dynamics, is small compared to the interval ($\zeta_D - \zeta_C$) during which the slow dynamics operates, in turn giving way to the fast level change from D to E. The interval corresponding to the latter is obtained as a sum of two sub-intervals : (a) the interval necessary for $u(\zeta)$ to drop from $2a$ to a (point D' in fig. 7), and (b) the interval for $u(\zeta)$ to drop from a to $u_\zeta|_E \sim -1 + 2a$. However, in order to calculate these sub-intervals to the leading order in ϵ , one has to again perform a matching between the outer and the inner solutions, as was done for the point C. One thereby obtains

$$\zeta_E - \zeta_D \sim 2\frac{\ln\epsilon}{\ln\sigma}. \quad (48)$$

Finally, the slow dynamics takes over from E onwards, and the pulse returns to the level $u = 0$, $w = 0$ over an infinite ζ -interval.

Summarising, we present below the travelling pulse solution obtained in the leading order of singular perturbation calculation:

$$-\infty < \zeta < \zeta_C : \quad u(\zeta) \sim g(\zeta), \quad (49a)$$

$$w(\zeta) \sim \frac{\epsilon}{\chi} \int_{-\infty}^{\zeta} g(\zeta) d\zeta, \quad (49b)$$

$$\zeta_C < \zeta < \zeta_D : \quad u(\zeta) \sim e^{-\frac{\epsilon}{\chi}(\zeta - \zeta_C)}, \quad (49c)$$

$$w(\zeta) \sim 1 - e^{-\frac{\epsilon}{\chi}(\zeta - \zeta_C)}, \quad (49d)$$

$$\zeta_D < \zeta < \zeta_E : \quad u(\zeta) \sim 2a - g\left(\zeta - \frac{\zeta_E + \zeta_D}{2}\right), \quad (49e)$$

$$w(\zeta) \sim 1 - 2a, \quad (49f)$$

$$\zeta_E < \zeta < \infty : \quad u(\zeta) \sim -(1 - 2a)e^{-\frac{\epsilon}{\chi}(\zeta - \zeta_E)}, \quad (49g)$$

$$w(\zeta) \sim (1 - 2a)e^{-\frac{\epsilon}{\chi}(\zeta - \zeta_E)}, \quad (49h)$$

where ζ_C , ζ_D , ζ_E have been obtained above (see equations (46), (47), (48)). Note that in this pulse solution the matching of $u(\zeta)$ as also of $w(\zeta)$ at ζ_C , ζ_D , and ζ_E is accurate only in the leading order in ϵ , and so are the values of ζ_C , ζ_D , ζ_E themselves.

Fig. 8 shows an initial ($t = 0$) pulse profile constructed in accordance with eq. (49a) - (49h) as also the profile obtained by numerical integration of (31a), (31b) with this initial condition for a time lapse τ (see caption). At the same time, it depicts the profile obtained from (49a) - (49h) by putting $t = \tau$. The agreement of the latter two indicates that (49a) - (49h) does indeed constitute a travelling pulse solution of (31a), (31b).

On the other hand, when a similar exercise is performed (fig. 9) with a pulse constructed as in (49a) - (49h) but with matchings done at ζ -values deviating from those in (46)- (48) (we use changed values $\zeta'_C = 2\zeta_C$, $\zeta'_D - \zeta'_C = \zeta_D - \zeta_C$, $\zeta'_E - \zeta'_D = 2(\zeta_E - \zeta_D)$), one observes that the profile at $t = \tau$ differs markedly from that obtained by numerical integration of the initial profile for a time lapse τ , thereby confirming the validity of our singular perturbation construction.

C. The periodic pulse-train

Similar principles can be used to construct a one-parameter family of travelling *pulse-trains* where a pulse-train involves a periodic succession of pulses travelling along the lattice with a constant speed. Whereas a lone pulse involves a leading edge with a level change (from $u = 0$ to $u = 1$) at $w = 0$ and a trailing edge with a level change (from $u = 2a$ to $u = -1 + 2a$) at $w = 1 - 2a$, the leading edge of each pulse in a pulse train involves a level change at some non-zero value (say, W) of the recovery variable w . where W is to lie in the range $0 < W < \tilde{a} - a$ where the upper limit is obtained by noting that a kink solution with its level change occurring at $w = \tilde{a} - a$ gets pinned in the lattice.

Fig. 10 depicts schematically the variation of u_0 with t where successive level changes occur with alternating fast and slow dynamics, the points of matching between the inner and outer solutions being shown in a manner similar to fig. 6. Note that the leading edge of each pulse, instead of rising from $u_0 = 0$, joins up with the trailing edge of the previous pulse in the pulse train and thus, for each pulse in the train there are four matching points (C, D, E, F in fig. 10) instead of three (cf. fig. 6) for a lone pulse. Fig. 11 shows the pulse train

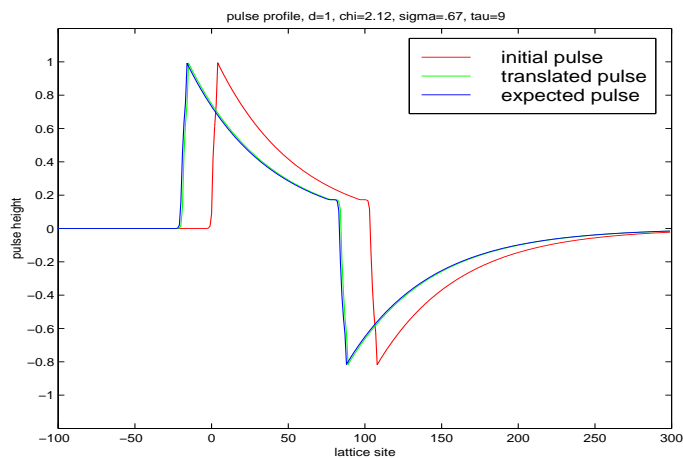


FIG. 8: An initial profile obtained from the theoretically calculated pulse solution with $t = 0$, together with the profile (‘translated pulse’) obtained from the initial profile on numerical integration of the FitzHugh-Nagumo system for a time lapse τ , and the theoretically calculated profile drawn with $t = \tau$ (‘expected pulse’); $D = 1, \epsilon = .04, \sigma = 0.67, a = 0.0864, \tau = 9$; the translated and expected pulses coincide in the scale of the figure.

dynamics in the $u_0 - w_0$ phase plane where the closed curve is traversed repeatedly, and the matching points together with the points of threshold crossing are indicated.

Applying the matching principles explained for the lone pulse, we obtain the pulse train solution as below (as explained above, we have a 1-parameter family of such solutions characterised by W):

$$-\zeta_1 < \zeta < \zeta_1 : \quad u(\zeta) \sim g(\zeta) - W, \quad (50a)$$

$$w(\zeta) \sim W, \quad (50b)$$

$$\zeta_1 < \zeta < \zeta_1 + \zeta_2 : \quad u(\zeta) \sim (1 - W)e^{-\frac{\epsilon}{\chi}(\zeta - \zeta_1)}, \quad (50c)$$

$$w(\zeta) \sim 1 - u(\zeta), \quad (50d)$$

$$\zeta_1 + \zeta_2 < \zeta < 3\zeta_1 + \zeta_2 : \quad u(\zeta) \sim 2a - g(\zeta - \zeta_1 - 2\zeta_2) + W, \quad (50e)$$

$$w(\zeta) \sim 1 - 2a - W, \quad (50f)$$

$$3\zeta_1 + \zeta_2 < \zeta < 3\zeta_1 + \zeta_2 + \zeta_3 : \quad u(\zeta) \sim -(1 - 2a - W)e^{-\frac{\epsilon}{\chi}(\zeta - 3\zeta_1 - \zeta_2)}, \quad (50g)$$

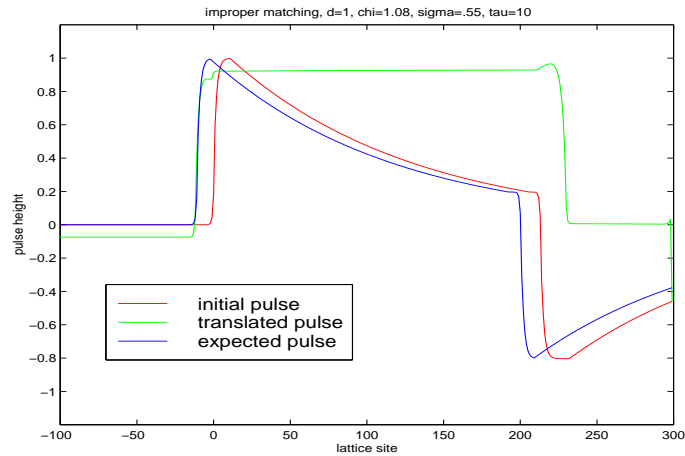


FIG. 9: Same as fig. 8, but with an improper matching between the fast and slow dynamics (see text); $D = 1, \epsilon = 0.009, \sigma = 0.5533, a = 0.0982, \tau = 10$.

$$w(\zeta) \sim -u(\zeta), \quad (50h)$$

$$u(\zeta + Z) = u(\zeta), \quad (50i)$$

$$w(\zeta + Z) = w(\zeta), \quad (50j)$$

where

$$\zeta_1 \sim \frac{\ln \epsilon}{\ln \sigma}, \quad (51a)$$

$$\zeta_2 \sim \frac{\chi}{\epsilon} \ln \left(\frac{1-W}{2a+W} \right), \quad (51b)$$

$$\zeta_3 \sim \frac{\chi}{\epsilon} \ln \left(\frac{1-W-2a}{W} \right), \quad (51c)$$

and the periodicity is

$$Z = 4\zeta_1 + \zeta_2 + \zeta_3. \quad (51d)$$

The speed χ of the pulse-train depends on the initial level W of the recovery variable and is given, in the leading order of ϵ , by the equation

$$\frac{1}{2\pi} \int_0^{2\pi} \frac{d\theta}{(1 - \nu \cos \theta)(1 - e^{-i\theta} e^{-\mu(1 - \nu \cos \theta)})} = -(2D + 1)(a + W - a_0) \quad (52)$$

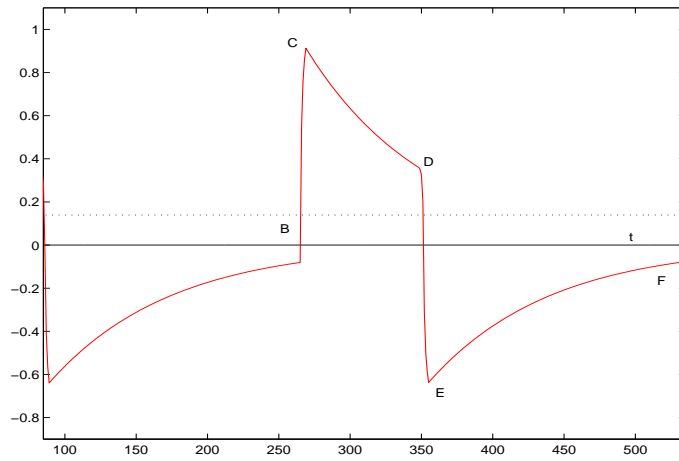


FIG. 10: u_0 as a function of t for a typical pulse-train solution showing schematically the matching points (similar to fig. 6); the trailing edge of one pulse joins up with the leading edge of the next pulse, and thus there are an infinite succession of matching points.

(cf. eq. (26) of [4] giving the speed of the kink solution for $W = 0$).

Fig. 12 shows a pulse-train profile (a) at $t = 0$ and (b) at $t = \tau$ (see caption) obtained from (50a) - (50j), together with (c) the profile obtained by numerical integration of (31a), (31b) for a time lapse τ . The agreement between (b) and (c) indicates that the pulse-train solution obtained above is indeed a valid one. Additionally, fig. 13 shows the result of a similar exercise but now with an improper matching between the inner and outer solutions using ζ -intervals as in fig. 9. One observes here that the pulse-train profile at $t = \tau$ differs substantially from the result of numerical integration from the initial profile.

IV. CONCLUDING REMARKS

In summary, we have, in this paper, established the temporal stability of the travelling front solution (2a) - (6c) of the discrete reaction-diffusion system (1a), (1b) by way of estimating the stability multiplier and have constructed the travelling pulse as also a one-parameter family of pulse-train solutions for a system including a slow variation of the recovery parameter, through a leading order singular perturbation analysis. The travelling pulse consists of a leading edge and a trailing edge corresponding to levels $w = 0$ and $w = 1 - 2a$ of the recovery variable, and also intervals of slow dynamics as explained above. A pulse-train, on the other hand, is made up of a periodic succession of pulses with the

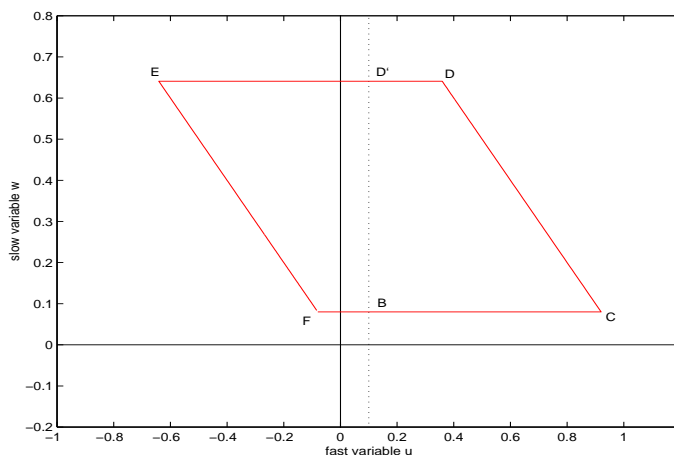


FIG. 11: u_0 - w_0 phase diagram for a pulse-train solution (similar to fig. 7); the closed loop is traversed periodically.

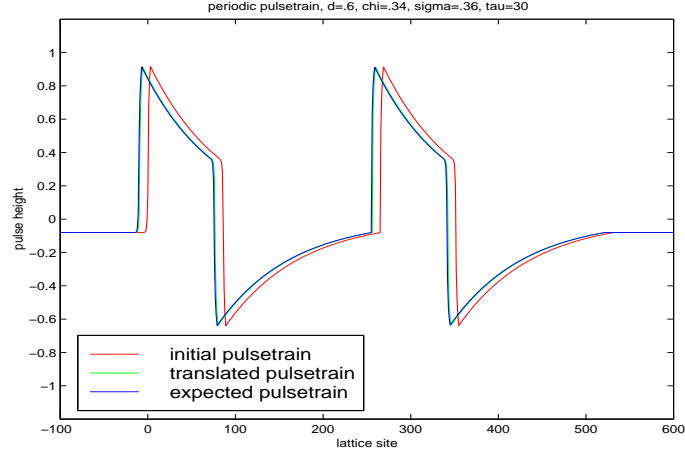


FIG. 12: Comparison of theoretically calculated and numerically computed pulse-train solution (similar to comparison in fig. 8 for a lone pulse); $D = 0.6, a = 0.1395, W = 0.08, \epsilon = 0.004, \tau = 30, \sigma = 0.3661$; once again, the ‘translated’ and ‘expected’ pulse trains coincide.

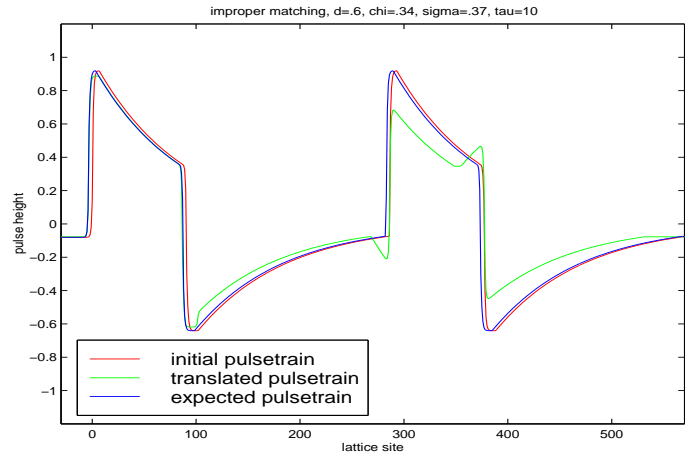


FIG. 13: Comparison of theoretically calculated and numerically computed pulse-train solution (similar to comparison in fig. 9 for a lone pulse), with an improper matching between the fast and slow dynamics (see text); parameters same as in fig. 12, but with $\tau = 10$.

leading edge of one pulse joined up with the trailing edge of the previous one. Each pulse-train solution belonging to the family is characterised by the parameter W , the value of the recovery variable at which the leading edge transition takes place (correspondingly, the trailing edge transition takes place at the value $(1 - 2a - W)$ of the recovery variable).

A periodic pulse-train is equivalent to a pulse propagating along a circular lattice, and can thus be used to model *re-entrant* pulses in a ring of excitable cells. Re-entrant waves have

recently been the focus of intense attention in understanding the origin of arrhythmias and fibrillations in the cardiac tissue, and are thought to constitute the mechanism underlying the break-up of spiral and scroll waves [16, 17, 18, 19].

In this context, we shall present, in a future communication, a stability analysis for the pulse solution following an approach adopted in [15]. There we consider the pulse to be travelling on a (sufficiently large) circular lattice (a pulse on a circular lattice is equivalent to a periodic pulse-train on a linear lattice; recall that a pulse-train is characterised by a parameter W) and reduce the problem of stability to that of obtaining the spectrum of a mapping in a function space. In deriving the stability criterion, we use a continuum version of (1a), (1b), while taking the lattice discreteness into consideration through the relation defining the speed χ of the pulse in terms of the parameter W , a special feature of this relation being the pinning of the pulse at $W = \tilde{a} - a$. We shall examine as to what extent the lattice discreteness with its attendant feature of pinning leads to a tendency of deviation from the so-called restitution hypothesis, the latter being a criterion of stability expressed in terms of the ‘diastolic interval’ (DI) and the ‘action potential duration’ (see, e.g., [14, 15, 20, 21]). In a separate communication we shall examine certain interesting features of pulse-train propagation on a discrete lattice in the presence of *pacemaker* oscillators, wherein the role of the pinning transition will be found to be especially crucial.

Acknowledgement: One of us (PM) acknowledges with thanks a research grant from CSIR, India, bearing sanction no. 8/463/Renewal/2004-EMR-I.

-
- [1] G. Fath, *Physica D* 116(1998)176-190 .
 - [2] J. Bell, *Math. Biosci.*, 4(1981)181
 - [3] J. Bell and C. Cosner, *Quart. Appl. Math.* 42(1984)1.
 - [4] A. Lahiri, P. Majumdar, and M. Sinha Roy, *Phys. rev. E*, 65(2002)026106.
 - [5] J. P. Keener, *SIAM J. Appl. Math* 47(1987)556.
 - [6] B. Zinner, *SIAM J. Math. Anal.* 22(1991)1016.
 - [7] B. Zinner, *J. Diff. Eqns.* 96(1992)1.

- [8] A. Hagberg and E. Meron, *Nonlinearity* 7(1994)805.
- [9] C. Conley, *Springer Lecture Notes in Physics*, vol. 38, Springer, Berlin (1987).
- [10] G. A. Carpenter, *J. Diff. Equations*, 23(1977)335.
- [11] S. P. Hastings, *SIAM J. Appl. Math.* 42(1982)247.
- [12] A. Lahiri, D. Goswami, B. Dasgupta, *Phys. Lett A* 108(1985)173.
- [13] K. Rajagopal, *Phys. Lett. A* 98(1984)49.
- [14] A. V. Panfilov, and C. W. Zemlin, *Chaos*, 12(2002)800.
- [15] E. Cytrynbaum, and J. P. Keener, *Chaos*, 12(2002)788.
- [16] A. V. Panfilov and J. P. Keener, *Physica D* 84(1995)545.
- [17] A. V. Panfilov and P. Hogweg, *Phys. Lett. A* 176(1993)295
- [18] A. V. Panfilov and A. Pertsov, *Phil. Trans. R. Soc. Lond.* 359(2001)1315.
- [19] A. V. Panfilov, *Chaos* 8 (1998)57.
- [20] A. Karma, H. Levine, and X. Zou, *Physica D* 73(1994)113.
- [21] M. Courtemanche, J. P. Keener, and L. Glass, *J. Appl. Math.*, 56(1996)119.